nature communications

Article

https://doi.org/10.1038/s41467-025-62113-1

A controllable photoresponsive potassium transporter

Received: 23 May 2024

Accepted: 10 July 2025

Published online: 28 July 2025

Check for updates

Zhongyan Li[1], Lin Yuan[2], Wenju Chang[1], Junqiu Liu[3], Jie Shen[1] ✉ & Huaqiang Zeng[1] ✉

Artificial photoresponsive transport systems are particularly intriguing because they offer the potential for precise spatio-temporal control, rapid response times and minimal toxicity associated with the light. We report here a controllable, photoresponsive, ion-transporting carrier, achieving controllability through a photoregulated β-cyclodextrin (β-CD)-azobenzene host-guest complex. In this complex, a lipid-anchored β-CD serves as the launch base, tightly immobilizing through host-guest interactions the otherwise freely moving trans-transporter derived from a crown ether-modified trans-azobenzene motif, but rapidly releasing most of it upon 365 nm UV irradiation that converts transporter to its cis-configuration. The launched cis-transporter functions well as a highly efficient potassium transporter, delivering a low EC_{50} value of 1.51 μM and a drastic transport activity enhancement by ~400% relative to the base-bound trans-transporter (EC_{50} = 7.46 μM), with on-off activities repeatedly regulated by light. In the absence of the base, the on-off activities between cis- and trans-transporters however differ by only 80% (1.35 μM vs 2.45 μM).

Regulating biological and cellular activities critically relies on channel proteins—cell's gatekeepers that enable selective passage of specific substances—to ensure proper transmembrane electrochemical gradients via precise control of ion homeostasis[1]. Understanding the structure, function, and regulation of these gatekeepers is essential for unraveling their role in physiological processes and their potential implications in health and disease. Aiming to mimic or even surpass the capabilities of natural channel proteins, artificial membrane transporters have emerged as a promising area of research at the intersection of chemistry, materials science and biotechnology[2–23].

Gated artificial membrane transporters offer a fascinating approach, where external stimuli such as temperature shifts, pH changes, ligand binding, voltage, redox variations, and light exposure are applied to modulate ion transport rates[19,20,24–29]. Among these stimuli, light offers strong appeal for its potential for biocompatible spatiotemporal control, rapid response time and minimal toxicity. Therefore, there has been long-standing interest in devising artificial membrane transporter systems, employing various photochromic groups to regulate ion transport across biological membranes[19,20,30–41]. Nevertheless, while photo-responsive host-guest chemistry has found wide uses in diverse supramolecular, material, biological and pharmaceutical applications across diverse fields[42,43], it has never been applied to control the reusability of ion transporters in any photoregulated artificial membrane transporters studied so far[19,20,29–41].

Combining concepts from host-guest chemistry and photochemistry and further building upon our enduring interest in developing transmembrane ion transporter system[21,44–48], we demonstrate here that a controllable photoresponsive transporter properly designed at the molecular level can be built to deliver on demand within the context of lipid bilayer membrane. In the presence of β-CD-mediated host-guest interactions, the light-triggered release of membrane-active transporter in its *cis*-configuration results in a drastic K^+ transport activity enhancement by ~400% relative to the β-CD-bound transporter in its *trans*-configuration, with on-off activities

[1]College of Chemistry, Fuzhou University, Fuzhou, Fujian, China. [2]College of Chemistry and Bioengineering, Hunan University of Science and Engineering, Yongzhou, Hunan, China. [3]College of Material, Chemistry and Chemical Engineering, Key Laboratory of Organosilicon Chemistry and Material Technology, Ministry of Education, Hangzhou Normal University, Hangzhou, China. ✉e-mail: shenjie@fzu.edu.cn; hqzeng@fzu.edu.cn

repeatedly regulated by light. In the absence of host β-CD, the on-off activities between *cis*- and *trans*-transporters however differ by only 80%.

Results and discussion

Molecular design

The hydrophobic cavity of β-CD (Fig. 1a) binds *trans*-azobenzene more tightly than its *cis*- form (Fig. 1b)[49], providing an appealing type of photoresponsive host-guest interactions for building up membrane-active, light-regulated, controllable ion transporters (Fig. 1c). Functioning as the base, the host compound (**H**) was obtained by modifying β-CD molecule (**h**) with the important, indispensable, triply alkylated gallic acid-based lipid anchor (Fig. 1a and Supplementary Figs. 1, 2). This lipid anchor partitions β-CD-derived launch base into the amphiphilic membrane-water interface. And as will be discussed later, in its absence, the controllable concept does not work at all. The guest molecules, i.e., transporters **1**–**3**, consist of three modularly tunable parts: an azobenzene group that interacts with β-CD in a photo-responsive manner, a liposoluble flexible linker of varying lengths that enables part of the transporter to bend and flip, and an ion-loading and releasing 18-crown-6 group (Fig. 1b).

Structurally resembling the ion transporters that transport ions through a swimming-like mechanism[47] the ion transport cycle roughly comprises six steps (Fig. 1c). Initially, the transporter system involving base **H** and transporters **1**–**3** is on the off state, with the azo group of **1**–**3** in trans-configuration and bound by base **H**. In step 1, UV light irradiation at 365 nm converts *trans*- to *cis*-configuration, attenuating the host-guest interactions and hence launching the transporter into the membrane from the base to perform its ion-transporting task. These transporters will then move down the ion concentration gradient in step 2, flip using its flexible alkyl chain to release the ion in step 3 and to head up in step 4. Visible light-mediated photoisomerization in step 5 induces cis-azo into trans configuration, returning the transporter to the base in step 6 and awaiting the UV signal to start another transport cycle.

Host H can control the ion transport activity of *t*-3, but h cannot

As illustrated in Fig. 2a, we hypothesized that water-soluble β-CD (**h**) could be anywhere in solution or near the membrane, becoming less accessible to membrane-residing trans-transporter ***t*-3** for efficient binding and that the β-CD part of **H** will stay in the amphiphilic membrane region, which may greatly enhance its ability to bind the azo group ***t*-3**. In either case, it is well known[49] and further demonstrated here neither **h** nor **H** will strongly bind ***c*-3** (Table 1). We further believe the length of the alkyl chain from **3** may exert additional influences on the ability of **H** to recognize the azo group, given the surmise that the chain length must be appropriate for the azo group to reach inside the hydrophobic cavity of β-CD.

To test the above hypothesis and to quickly identify the best host-guest pair for achieving the highest controllability in ion transport

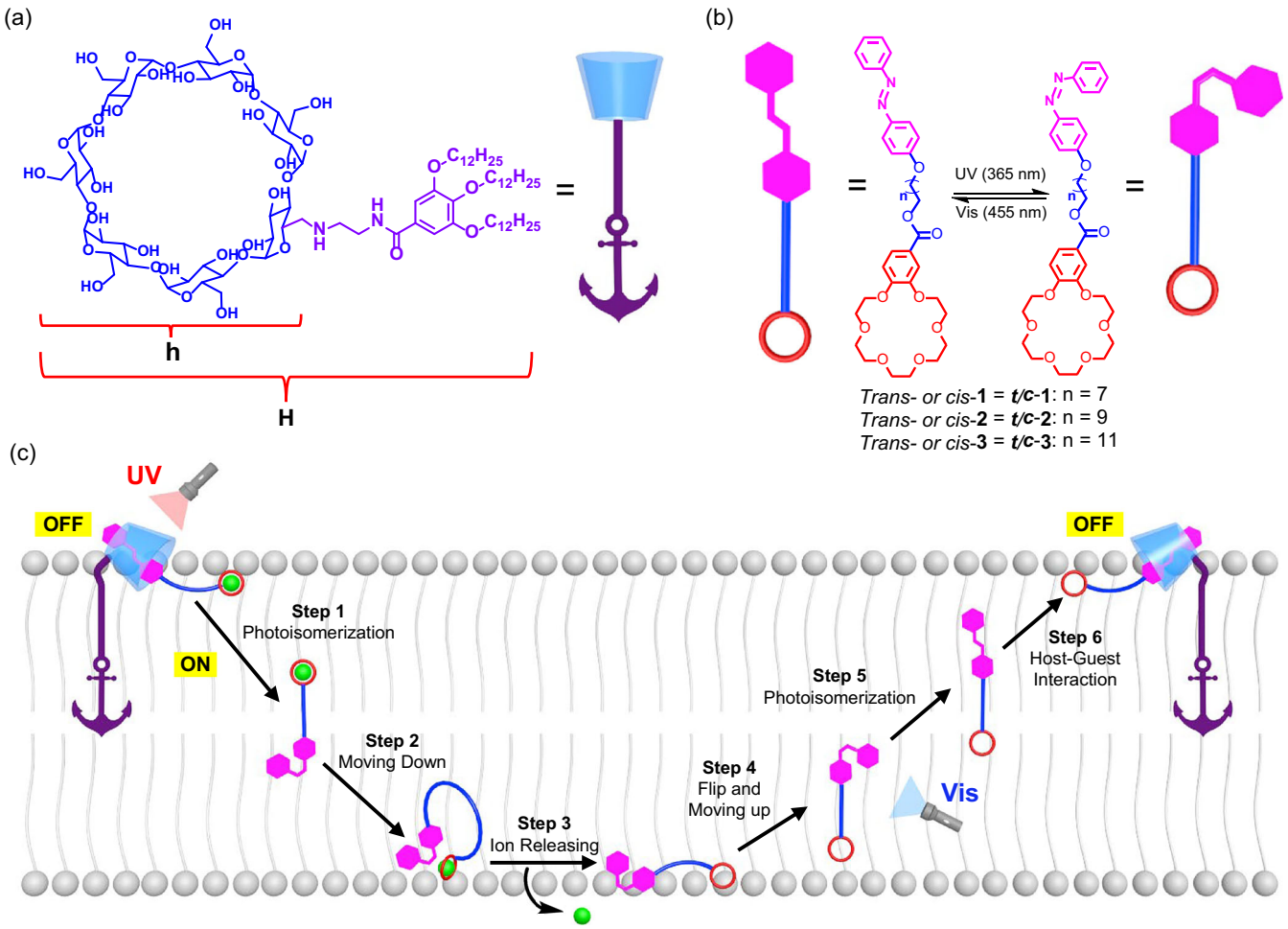

Fig. 1 | Possible working principle of potassium ion transporters. a, **b** illustrate molecular design and structures of hosts **h** and **H** as well as guest molecules **1**–**3**. **c** A schematic illustration of how an azo-benzene-derived molecular ion transporter might become controllable in the presence of lipid anchor-modified β-CD molecule through photoresponsive host-guest recognition. Note that step 5 can take place anywhere in the membrane. Based on the computed binding energies presented in Supplementary Fig. 15, the released *cis*-form likely binds K^+ to generate an intramolecular cyclic complex for facilitating K^+ transport.

https://doi.org/10.1038/s41467-025-62113-1

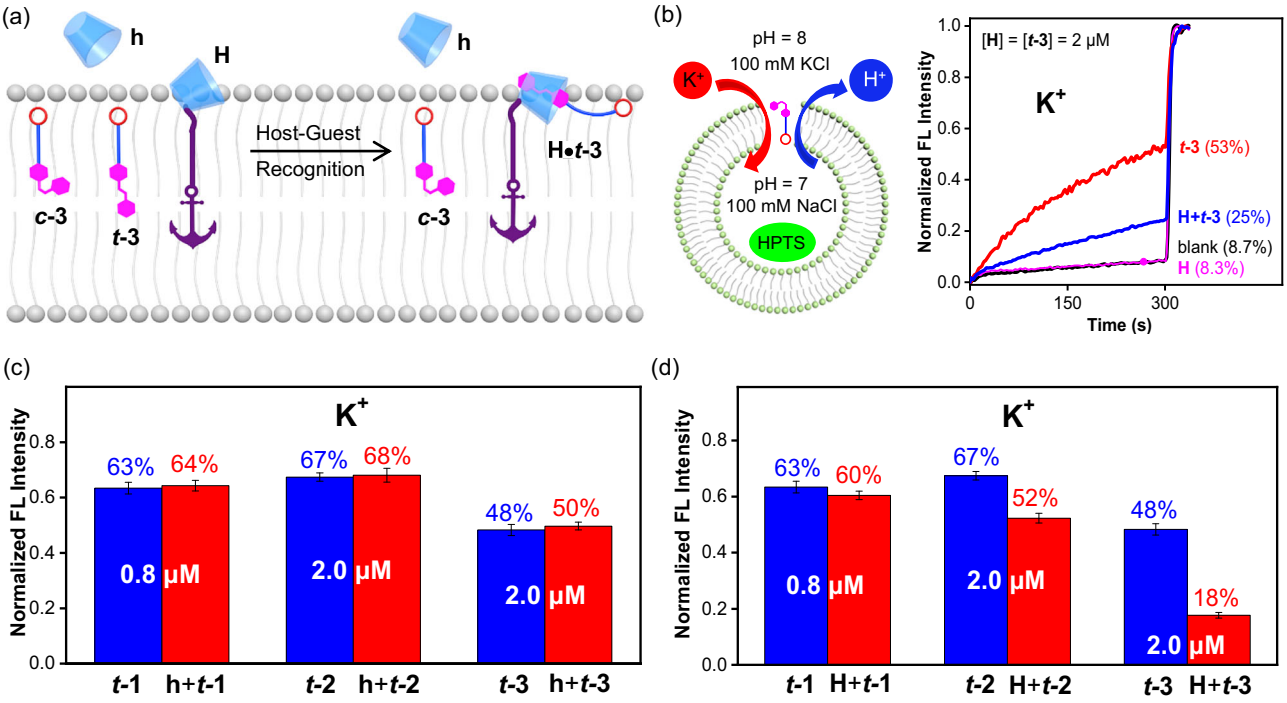

Fig. 2 | Host-guest dependent ion transport activities determination. a Mixing **h**, **H**, ***t*-3** and ***c*-3** generates only host-guest complex **H•*t*-3**. **b** The LUV-based pH-sensitive HPTS assay for evaluating ion transport activities of **3** at 2.0 μM; here, $R_{K^+} = (I_{K^+} - I_0)/(I_{Triton} - I_0)$ whereas I_{K^+} and I_0 are the ratiometric values of I_{460}/I_{403} at $t = 300$ s before addition of triton, and I_{Triton} is the ratiometric value of I_{460}/I_{403} at $t = 300$ s right after addition of triton. **c** The ion transport activities of ***t*-n** ($n = 1$–3) in the presence of host **h**. **d** The ion transport activities of ***t*-n** ($n = 1$–3) in the presence of host **H**. HPTS = 8-Hydroxypyrene-1,3,6-trisulfonic acid trisodium salt. All data represent mean ± SD from three independent experiments ($n = 3$).

Table 1 | The binding constants between guests (*t*-n and c-3) and hosts (h and H) in MeOH or lipid-containing buffer solutions[a]

	In MeOH		In lipid-containing buffer	
	h	H	h	H
***t*-1**	7.5×10^3	7.8×10^3	n.b.[b]	3.6×10^4
***t*-2**	5.3×10^3	1.5×10^4	n.b.[b]	8.6×10^4
***t*-3**	1.3×10^4	2.0×10^4	n.b.[b]	1.0×10^5
***c*-3**	1.0×10^4	6.0×10^3	n.b.[b]	1.5×10^3

[a]Buffer condition: 0.08 mM LUV in 100 mM NaCl, 10 mM HEPES and pH = 8.
[b]No binding detected.

activity, we applied a well-established pH-sensitive HPTS assay dye (Fig. 2b) to obtain the fractional ion transport activities for six combinations involving **h**, **H** and **1**–**3** in their *trans*-form at equal-molar mixing. First and importantly, lipid anchor- containing **H** hardly transports any ion at 2.0 μM. Second, having the longest 12 carbon atom alkyl chain, ***t*-3** displays the greatest normalized differential activities of 48% (e.g., (53%−8.7%/91.3%)) and 18% in the absence and presence of host **H** at [***t*-3**] = [**H**] = 2.0 μM (Fig. 2b). This confirms that the *β*-CD fragment in **H** can bind membrane-residing ***t*-3**, decreasing its transport activity by >60%. In sharp contrast, host **h**, having no lipo-soluble lipid anchor, weakly binds any transporter molecule ***t*-n** ($n = 1$–3) since no differences in transport activity are recorded for ***t*-n** in the absence and presence of host **h** (Fig. 2c). This finding clearly indicates that binding behaviors observed in solutions are not necessarily extendable into membrane-water interface, and they are distinctively different. Third, the ion transport activities of ***t*-1** to ***t*-3** in the presence of **H** inversely correlates with the increasing alkyl chain lengths, pointing to increasingly stronger binding of ***t*-1** to ***t*-3** by **H**. For ***t*-1** and ***t*-2** to reach 50% decrease in activity, the concentration of **H** needs to be 5 and 2 times that of the transporter (Supplementary Fig. 6), respectively. In brief, although ***t*-1** exhibits the highest transport activity, it is ***t*-3** that binds **H** the strongest, which is the most important prerequisite to consider in designing controllable transporters.

Binding constants between hosts (h and H) and guests (1-3)

To shed some light on the observed transport activities, we have determined the binding constants between four azobenzene-containing guests (***t*-1**, ***t*-2**, ***t*-3** and ***c*-3**) and two CD-derived hosts (**h** and **H**) in MeOH and in a lipid-containing buffer solution (e.g., blank vesicles, see: Table 1, Supplementary Figs. 8, 9 and Supplementary Tables 2, 3).

First, all the measured binding constants align well with the experimental data on ion transport activity presented in Fig. 2b–d. Particularly, the binding affinities between the *trans*- and *cis*-transporter **3** and the lipid-anchor-modified *β*-CD host **H** differ significantly by 67 times in LUVs ($1.0 \times 105\ M^{-1}$ for ***t*-3** vs. $1.5 \times 103\ M^{-1}$ for ***c*-3**). As a result, the conversion of ***t*-3** to ***c*-3** by 455 nm light irradiation should release more active ***c*-3** from the **H•*t*-3** complex, which in turn increases ion transport activity. This provides a strong basis to support the concept behind the controllable photoresponsive transporter model.

Second, it is noteworthy that host **h** binds similarly to ***t*-n** guests in MeOH containing up to 40% H_2O (Table 1 and Supplementary Table 2) compared to the lipid anchor-containing **H**. However, this trend does not hold true in the lipid-containing buffer solution, where no binding is observed between **h** and ***t*-n**, while high binding constants of $(0.36 - 1.0) \times 10^5\ M^{-1}$ is observed between **H** and ***t*-n**, confirming that lipid-residing **H** is more accessible to ***t*-n** in lipid than solution-residing **h**. This is consistent with the ion transport activity of ***t*-n** in the presence of either host (Fig. 2c, d). Specifically for ***t*-3**, the presence of **h** has no effect on its ion transport activity in the lipid-containing buffer

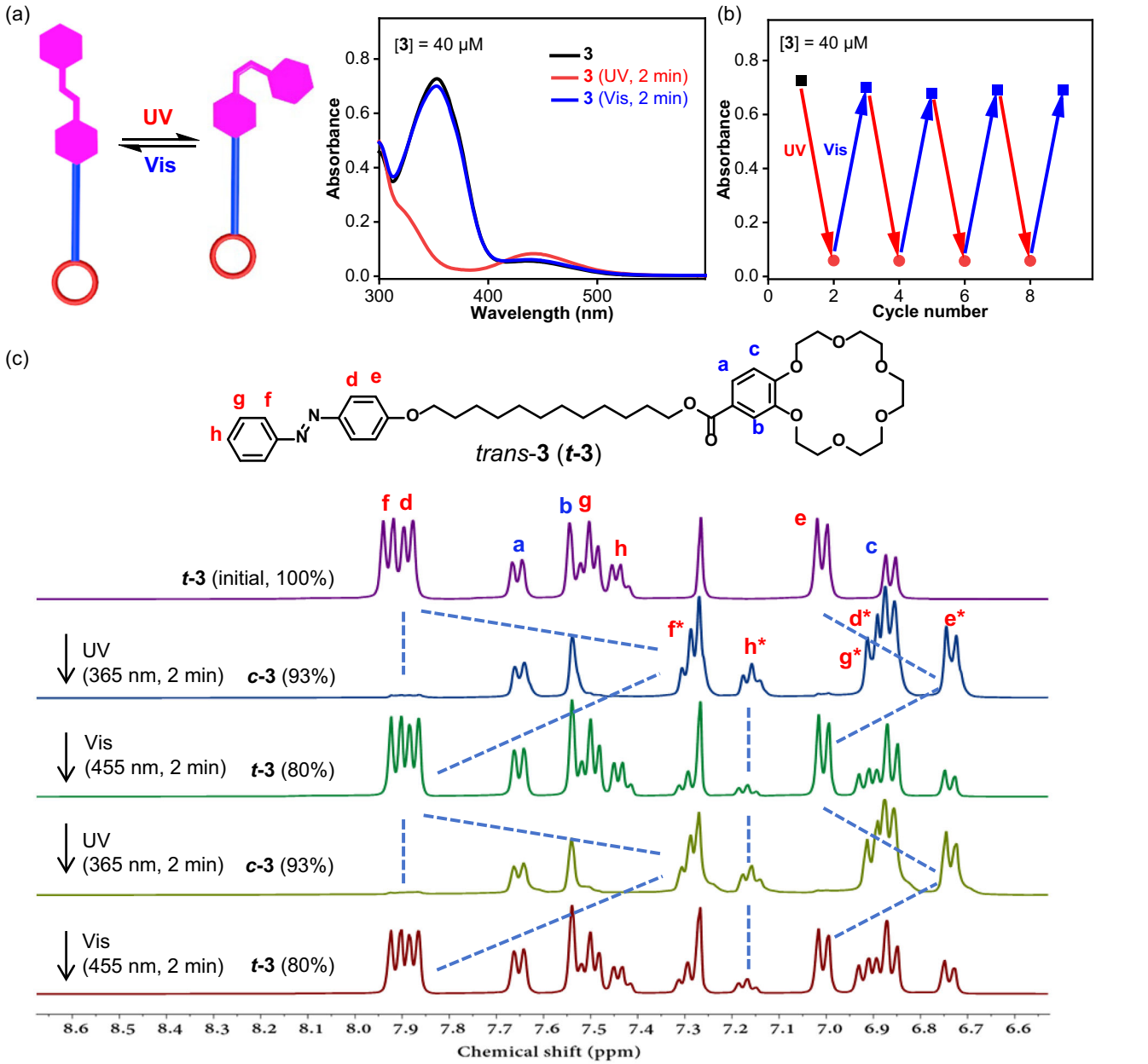

Fig. 3 | Study on the optical properties of transporter 3. a UV spectra of **3** under alternative UV and Vis light irradiation, suggesting photoisomerization mostly completes within 2 min. **b**, **c** show multiply cycled UV and ^{1}H NMR spectra of **3** at 13 mM in $CDCl_3$ demonstrating the photoisomerization to be a reversible process.

solution, whereas **H** reduces its unnormalized ion transport activity from 53% to 25% (Fig. 2b).

3 reversibly isomerizes with or without H under alternating light irradiation

With the host-guest complex **H•*t*-3** demonstrated to function within the context of lipid membrane and have a desired binding constant much higher than that of **H•*c*-3**, we conducted UV and ^{1}H NMR on **3** to check its photo property (Fig. 3). **3** was synthetically obtained in its trans-form, i.e., ***t*-3**, and undergoes rapid structural isomerization to its *cis*-form ***c*-3** after exposure to UV light at 365 nm for 2 min (Fig. 3a and Supplementary Fig. 10). Subsequent irradiation using visible light at 455 nm rapidly regenerates ***t*-3**. Extending irradiation to 5 min has no influence on the reversible isomerization efficiencies (Supplementary Fig. 11). Further ^{1}H NMR-based study (Supplementary Fig. 12) gives the photochemical quantum yields of 37.2% and 47.2% under 365 nm and 455 nm light sources, respectively, and the experimental details and process can be found in Supplementary Fig. 12 and Supplementary Information. This photoisomerization can reversibly take place under alternative UV and visible light irradiation (Fig. 3b). In addition, the effect of vesicles on the photoisomerization of azo group was determined using HPLC analysis and compared to those in MeOH, and the results show that lipid molecules do not exert significant influence on the isomerization extent of azobenzene group (Supplementary Table 3 and Supplementary Figs. 13 and 14).

^{1}H NMR investigations reveal very substantial upfield shifts of protons H_f, H_h and H_e to protons H_{f^*}, H_{h^*} and H_{e^*} after UV light irradiation. Subsequent exposure to visible light returns these three protons to where they should be (Fig. 3c). This ^{1}H NMR study also confirms the isomerization of azo group to be reversible. Based on the relative peak intensities of H_a, H_d, H_e and H_f, the isomerization efficiencies of ***t*-3** to ***c*-3** and of ***c*-3** to ***t*-3** were calculated to be 93% for and 80%, respectively. The fact that the chemical shifts of protons *a*-*c* remain

https://doi.org/10.1038/s41467-025-62113-1

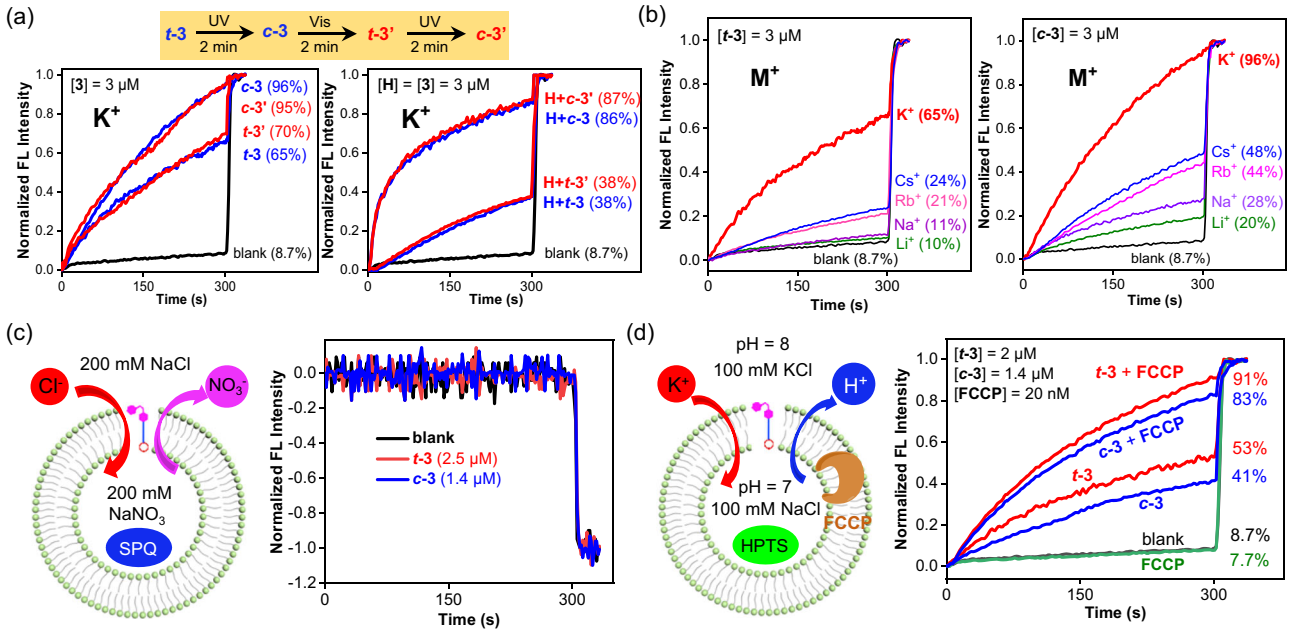

Fig. 4 | Exploration of potassium ion transport mechanism. a K^+ transport activities of **3** under alternative UV and Vis light irradiations, supporting the notion that reversible photoisomerization is independent of **H**. **b** Ion transport selectivity of ***t*-3** and ***c*-3** determined by varying the extravesicular MCl salts; here, $RM^+ = (I_{M^+} - I_0)/(I_{Triton} - I_0)$ whereas I_{M^+} and I_0 are the ratiometric values of I_{460}/I_{403} at $t = 300$ s before addition of triton, and I_{Triton} is the ratiometric value of I_{460}/I_{403} at $t = 300$ s right after addition of triton. **c** The chloride-sensitive SPQ assay, employing SQP dye whose fluorescence is quenched by Cl^- anions and demonstrating **3** does not transport Cl^-. **d** The HPTS assay in the presence of proton carrier FCCP, confirming **3**-mediated K^+ transport rate to be faster than H^+. SPQ 6-Methoxy-N-(3-sulfopropyl)quinolinium, FCCP carbonyl cyanide-p-trifluoromethoxyphenylhydrazone.

unchanged before and after light exposure suggests that azo group does not interact strongly with the benzo-crown ether group.

Using the same HPTS assay shown in Fig. 2b, ion transport activity of **3** was found to proceed reversibly between ***t*-3** and ***c*-3** upon alternating light irradiation at 365 and 465 nm (Fig. 4a). And such reversibility in activity is maintained in the presence of host **H**.

3 transports K^+ ions selectively

By varying the extravesicular metal chlorides from LiCl to CsCl, the ion selectivity for both ***t*-3** and ***c*-3** (each at 3 μM) was found to follow the same trend, with transport activity increasing in the order $Li^+ < Na^+ < Rb^+ < Cs^+ < K^+$ (Fig. 4b). In terms of overall activity, ***c*-3** exhibits greater transport efficiency than ***t*-3**.

To elucidate why ***c*-3** is more active than ***t*-3**, we examined their structural and binding characteristics. We initially employed the well-established picrate extraction method developed by Cram[50] to determine the binding constants of both ***t*-3** and ***c*-3** for Li^+, Na^+, K^+, Rb^+ and Cs^+ ions (Supplementary Table 5). For both ***t*-3** and ***c*-3**, the measured binding constants follow the same trend $K^+ > Rb^+ > Cs^+ > Na^+ > Li^+$, which largely aligns with the ion transport selectivity observed in Fig. 4b. Notably, ***c*-3** exhibits a 23% stronger binding affinity for K^+ than ***t*-3** (1.79×10^4 M^{-1} for ***c*-3** vs. 1.46×10^4 M^{-1} for ***t*-3**), which is in excellent agreement with its enhanced K^+ transport activity.

Subsequently, we calculated their binding energies with K^+ in four distinct binding modes **A**–**D**, corresponding to monomeric extended, intramolecular cyclic, head-to-tail dimeric, and head-to-tail polymeric, respectively (Supplementary Fig. 15). Our calculations show that ***t*-3** and ***c*-3** bind K^+ with no significant difference in monomeric extended binding mode **A**. However, in binding modes **B**–**D**, ***c*-3** exhibits binding energies approximately 3–6 kcal/mol higher than those of ***t*-3**, indicating a stronger binding affinity of ***c*-3** toward K^+ ion. This finding is consistent with its higher ion transport activity and greater binding constant compared to ***t*-3**. Moreover, ***c*-3** in its intramolecular cyclic binding mode **B** emerges as the most stable among binding modes **A**–**D**. The corresponding cyclic complex [***c*-3**•K^+•H_2O] exhibits a binding energy of −72.8 kcal/mol, which is more stable than modes **A**, **C** and **D** by 10.3, 3.5 and 10.9 kcal/mol, respectively. These results indicate that the enhanced K^+ transport by ***c*-3** is likely mediated via the formation of an intramolecular cyclic complex.

Finally, we conducted molecular dynamics (MD) simulations to analyze the movement of ***t*-3** or ***c*-3** within the membrane (Supplementary Fig. 16). Using the distance from the molecular centroid of either ***t*-3** or ***c*-3** to the membrane center along the *Z*-axis as the mobility indicator, we observed distinct behaviors. ***t*-3** predominantly oscillates near the membrane center, while ***c*-3** exhibits a pronounced tendency to migrate toward the membrane's hydrophilic region. These findings are in accord with the observed higher ion transport activity of ***c*-3** compared to ***t*-3**. Collectively, this higher mobility within the membrane, combined with its stronger K^+-binding affinity, contributes to ***c*-3**'s enhanced ion transport rate by relative to ***t*-3**.

The inability of ***t*-3** and ***c*-3** to transport anions was established through the SPQ assay (Fig. 4c). This assay is dependent on the capacity of Cl^- to quench the fluorescence emitted by the SPQ dye. Therefore, the finding that both ***t*-3** and ***c*-3** yield fluorescence readings mirroring background levels strongly indicates their incapability to prompt a measurable influx of Cl^- ions.

Considering that (1) alterations in HPTS fluorescence intensity are predominantly influenced by H^+ or OH^- but not Cl^-, and (2) ***t*-3** and ***c*-3** do not facilitate anion transport, the influx of K^+ mediated by ***t*-3** and ***c*-3** should undergo compensation via H^+ efflux through passive membrane diffusion to uphold the system's charge neutrality. To evaluate the transport rates of K^+ in comparison to H^+, HPTS assay was carried out in the presence of 20 nM FCCP (a potent of H^+, the introduction of FCCP would amplify the efflux of accumulated H^+, causing notable increments in fluorescence intensity. Indeed, the addition of FCCP at 20 nM results in a 38% increase (from 53% to 91%) for ***t*-3** at 2 μM and 41% increase (from 42% to 83%) for ***c*-3** at 1.4 μM, confirming the rate of K^+ transport to be higher than that of H^+.

To eliminate the potential influence of **3**-induced membrane disruption on the observed ion transport activities, we evaluated

https://doi.org/10.1038/s41467-025-62113-1

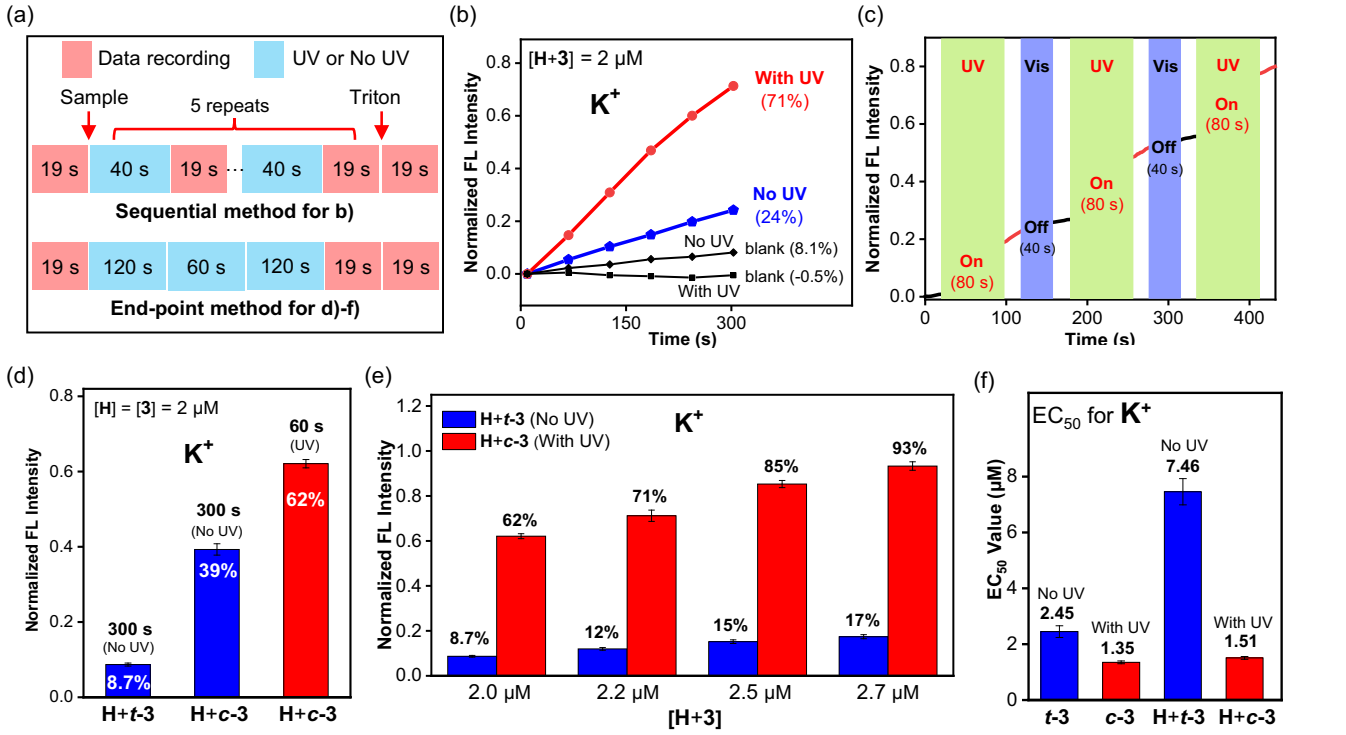

Fig. 5 | Determination of potassium ion transport performance. a Sequential and End-point methods for evaluating ion transport activities of **3** shown in (**b**) and (**d**)–(**f**), respectively, with a slightly different sequential method presented in Supplementary Fig. 4 for obtaining data shown in (**c**). **b** K^+ transport activity of **3** in the presence of **H** under UV irradiation increases by 300% relative to that in the absence of light irradiation. **c** Light-triggered on-off regulation of **3**-mediated K^+ transport. **d3**-mediated K^+ transport activities at 2 μM in the presence of **H** in dark for 300 s or under UV irradiation for 60 s using the End-point method. **e** Comparative K^+ transport activities between **H** + ***t*-3** and **H** + ***c*-3** at different concentrations determined using the End-point method. **f** The EC_{50} values for ***t*-3**, ***c*-3**, **H** + ***t*-3** and **H** + ***c*-3** determined using the End-point method. All data represent mean ± SD from three independent experiments ($n = 3$).

membrane integrity through a CF dye assay (CF = 5(6)-carboxy fluorescein, Supplementary Fig. 17). The CF dye consists of two isomers with dimensions of 9.2 Å × 11.4 Å and 10 Å × 10 Å, respectively. Normally, CF molecules confined intravesicularly tend to self-dimerize at 50 mM, giving rise to weak fluorescence. However, when leaked into the extravesicular space, they experience partial dissociation, generating highly fluorescent monomers. Experimentally, ***t*-3** at 4 μM and ***c*-3** at 2 μM showed no notable increase in fluorescence compared to a blank control. Conversely, pore-forming melittin molecules at 0.2 μM exhibit a substantially heightened normalized fluorescence intensity of 92%. Hence, these findings validate the integrity of the membrane in the presence of **3**, or at the very least, indicate that any pores formed by **3** were smaller than 1 nm in diameter.

c-3 transport K^+ ions 5 times as fast as *t*-3 in the presence of H

All above LUV-based experiments were conducted using the standard continuous method, having HPTS emission monitored at 510 nm upon alternate excitations at 460 and 403 nm every 1.7 s for a period of 300 s at constant temperature of 25 °C. To maximally eliminate the possible structural isomerization of azo-group by these light excitations, we have revised the normal procedure by introducing two alternative methods, i.e., sequential and end-point methods.

The sequential method comprises seven 19 s data collection blocks separated by five 40 s blocks with or without UV irradiation (Fig. 5a). The activity data collected during the 19 s blocks before adding sample and after adding triton to lysate the LUVs are set as 0% and 100%, respectively. For every 19 s block, 9 measurements were recorded, which were averaged to give a single data point, thereby leading to a total of six data points that are plotted against time to give the activity curves presented in Fig. 5b.

After normalization based on the background activity values, the K^+ transport activities of **H** + **3** (e.g., **3** in the presence of **H**) at 2 μM were 17% and 71% for **H** + ***t*-3** (No UV, Fig. 5b) and **H** + ***c*-3** (with UV, Fig. 5b), respectively. An activity increase by >300% under UV light irradiation validates our conceptual hypothesis underlying molecular design of controllable ion transporter. Explicitly, ***t*-3** gets tightly bound by the base **H** to form a host-guest complex **H**•***t*-3**, limiting the movability of ***t*-3** in the membrane. Upon UV light excitation that converts azo-group from its *trans*- to *cis*-configurations (e.g., from ***t*-3** to ***c*-3**), ***c*-3** was launched into the membrane, moving more freely to efficiently transport ions across the membrane.

To establish the controllability of ion transporter, a similar sequential method was employed (Fig. 5c). Here, "on" and "off" refer to 80 s exposure to UV light and 40 s exposure to Vis light, respectively, followed by collecting data for 19 s (Supplementary Fig. 4). Our results show that continued increases in ion transport activity during the "on" period flattens off when it reaches the "off" period. And this "on-off" operation can be repeated multiple times. These findings undoubtedly support the notion that the ion transport activity can be controlled in the presence of the base.

For the end-point method, there are three 19 s blocks for data collection, yielding only one end activity value rather than an activity curve (Fig. 5a). In between the 1st and 2nd 19 s blocks, transporters ***t*-3** or ***c*-3** in the presence of **H** at 2 μM was subject to either no UV treatment for 300 s or UV irradiation for 60 s or 300 s (Fig. 5d). The recorded activity data show that UV irradiation for 60 s (e.g., **H** + ***c*-3**) enhances the transport activity by up to 600% relative to that of **H** + ***t*-3**, and that a shorter UV exposure time of 60 s additional increases the activity by about 60% compared to a longer 300 s exposure time. Fixing the exposure time to 60 s, the activity values of **H** + ***c*-3** at

2.0–2.7 μM were determined to be 5.4–7.1 times those of **H** + ***t*-3**. (Fig. 5e)

Applying the Hill analysis, we obtained the EC_{50} values of 2.45 and 1.35 μM for ***t*-3** and ***c*-3** (Fig. 5f and Supplementary Fig. 18), respectively. Considering an isomerization efficiency of 93% for ***t*-3** to ***c*-3** and assuming such an efficiency is maintained in the membrane, EC_{50} value of ***c*-3** can be estimated to be 1.31 μM. That is, the activity of crown ether-containing **3** in its *cis*-form is about 1.9 times that of its *trans*-form. However, the presence of host **H** delightedly diminish the EC_{50} value of ***t*-3** from 2.45 μM to 7.46 μM while those for ***c*-3** are mostly the same (1.31 μM vs. 1.51 μM), thereby boosting the activity difference from 1.9 folds between ***t*-3** and ***c*-3** further to 5 folds between **H** + ***t*-3** and **H** + ***c*-3**.

Controllable transport with vs. without the base

Given that **3** itself can switch between ***t*-3** and ***c*-3** under alternating light irradiation, then, what is the benefit of having the β-CD base? As far as our concern, there are at least two key benefits to gain. Specifically, having the base to tightly lock the transporter can further (1) decrease the ion transport activity of undesired ***t*-3** by 2 folds (e.g., 2.45 μM down to 7.46 μM in EC_{50} value) and (2) enlarge the ion transport activity difference between undesired ***t*-3** and desired ***c*-3** (1.9 and 5 folds in the absence and presence of the base, respectively). These differences can be important such as to minimize the toxicity in medical treatment for which artificial ion transports play an important role. Another possible medicinal benefit of having the base is to lock the transporter ***t*-3** into the extracellular region, limiting its entry into the membrane of organelles (nucleus, mitochondria, lysosomes, etc). Through continued refinement in structure, we believe it is possible to additionally decrease the activity of the bound transporter while enlarging the activity difference between the bound and free transporter even further.

To summarize, we demonstrate that introducing host-guest chemistry into a photoresponsive ion transporter system allows for the successful construction of a controllable ion transporter, which can be launched on demand while exhibiting very substantial activity enhancement. This is achieved by pairing a lipid anchor-modified β-CD, which serves as the host and the base, with an azobenzene group-modified ion transporter, which functions as the guest. One important key to such success is the modification of the β-CD using a lipo-soluble lipid anchor, anchoring the β-CD into the amphiphilic membrane-water interface so that it can readily bind the lipo-soluble guest molecule. Subsequent alternating light irradiation using 365 nm UV and 455 nm visible lights triggers *trans-cis* isomerization of azo group, enabling light-regulated on-off host-guest interactions between the base and the transporter. This leads to the launch of transporter from the base upon 365 nm UV irradiation and its landing to the base after exposure to 455 nm visible light. Aside from this conceptual advancement, the ion transport activity difference between trans- and cis-transporters is substantially enlarged from ~2 folds in the absence of the base to 5 folds in its presence, offering a strategy that may impact the use of azo-benzene group in diverse fields.

Methods

Ion transport study using the HPTS assay and EC50 measurements using the Hill analysis. Egg yolk L-α-phosphatidylcholine (EYPC, 1 mL, 25 mg/mL in $CHCl_3$, Avanti Polar Lipids, USA) was added into a round-bottom flask. The solvent was removed under reduced pressure at 30 °C. After drying the resulting film under high vacuum overnight, the film was hydrated with the HEPES (4-(2-hydroxyethyl)-1-piperazine-ethane sulfonic acid) buffer solution (1 mL, 10 mM HEPES, 100 mM NaCl, pH = 7.0) containing pH sensitive dye HPTS (8-hydrox-ypyrene-1,3,6-trisulfonic acid, 1 mM) at room temperature for 60 min to give a milky suspension. The mixture was then subjected to 10 freeze-thaw cycles: freezing in liquid N_2 for 1 min and heating in 55 °C water bath for 2 min. The vesicle suspension was extruded through polycarbonate membrane (0.1 μm) to produce a homogeneous suspension of large unilamellar vesicles (LUVs) of about 120 nm in diameter with the HPTS encapsulated inside. The unencapsulated HPTS dye was separated from the LUVs by using size exclusion chromatography (stationary phase: Sephadex G-50, mobile phase: HEPES buffer with 100 mM NaCl) and diluted with the mobile phase to yield 5 mL of 6.5 mM lipid stock solution.

The HPTS-containing LUV suspension (25 μL, 6.5 mM in 10 mM HEPES buffer containing 100 mM NaCl at pH = 7.0) was added to a HEPES buffer solution (1.95 mL, 10 mM HEPES, 100 mM MCl at pH = 8.0, where $M^+ = Li^+$, Na^+, K^+, Rb^+ and Cs^+) to create a pH gradient for ion transport study. A solution of transporter molecules in DMSO was then injected into the suspension under gentle stirring. Upon the addition of transporters, the emission of HPTS was immediately monitored at 510 nm with alternate excitations at 460 and 403 nm for 300 s using fluorescence spectrophotometer after which time an aqueous solution of Triton X-100 (20 μL, 20% v/v) was immediately added to achieve the maximum change in dye fluorescence emission. The final transport trace was obtained, after subtracting background intensity at $t = 0$, as a ratiometric value of I_{460}/I_{403} and normalized based on the ratiometric value of I_{460}/I_{403} after addition of triton. The fractional changes R_{K^+} was calculated for each curve using the normalized value of I_{460}/I_{403}, with ratiometric value of I_{460}/I_{403} at $t = 0$ s as 0% and that of I_{460}/I_{403} at t = 300 s (obtained after addition of triton) as 100%. Fitting the fractional transmembrane activity RK+ vs transporter concentration using the Hill equation: $Y = 1/(1 + (EC_{50}/[C])^n)$ gave the Hill coefficient n and EC_{50} values.

The details of methods for the synthesis of **H** and transporter **1**–**3** was provided in Supplementary Information.

Data availability

Experimental details, procedures, spectra, crystallographic, and computational details are provided in the Supplementary Information file. The datasets that support the finding of this study are available in figshare repository with the identifier(s) https://doi.org/10.6084/m9.figshare.27188439. All data are available from the corresponding author upon request.

References

1. Suh, K. S. & Yuspa, S. H. Intracellular chloride channels: critical mediators of cell viability and potential targets for cancer therapy. *Curr. Pharm. Des.* **11**, 2753–2764 (2005).
2. Otis, F., Auger, M. & Voyer, N. Exploiting peptide nanostructures to construct functional artificial ion channels. *Acc. Chem. Res.* **46**, 2934–2943 (2013).
3. Montenegro, J., Ghadiri, M. R. & Granja, J. R. Ion channel models based on self-assembling cyclic peptide nanotubes. *Acc. Chem. Res.* **46**, 2955–2965 (2013).
4. Fyles, T. M. How do amphiphiles form ion-conducting channels in membranes? Lessons from linear oligoesters. *Acc. Chem. Res.* **46**, 2847–2855 (2013).
5. Huo, Y. P. & Zeng, H. Q. "Sticky"-ends-guided creation of functional hollow nanopores for guest encapsulation and water transport. *Acc. Chem. Res.* **49**, 922–930 (2016).
6. Chen, J.-Y. & Hou, J.-L. Controllable synthetic ion channels. *Org. Chem. Front.* **5**, 1728–1736 (2018).
7. Barboiu, M. Encapsulation versus self-aggregation toward highly selective artificial K+ channels. *Acc. Chem. Res.* **51**, 2711–2718 (2018).
8. Gong, B. Artificial water channels: inspiration, progress, and challenges. *Faraday Discuss.* **209**, 415–427 (2018).
9. Park, G. & Gabbaï, F. P. Phosphonium boranes for the selective transport of fluoride anions across artificial phospholipid membranes. *Angew. Chem. Int. Ed.* **59**, 5298–5302 (2020).

10. Davis, J. T., Gale, P. A. & Quesada, R. Advances in anion transport and supramolecular medicinal chemistry. *Chem. Soc. Rev.* **49**, 6056–6086 (2020).
11. Wu, X., Gilchrist, A. M. & Gale, P. A. Prospects and challenges in anion recognition and transport. *Chem* **6**, 1296–1309 (2020).
12. Zheng, S.-P., Huang, L.-B., Sun, Z. & Barboiu, M. Self-assembled artificial ion-channels toward natural selection of functions. *Angew. Chem. Int. Ed.* **60**, 566–597 (2021).
13. Yang, J. et al. Artificial transmembrane ion transporters as potential therapeutics. *Chem* **7**, 3256–3291 (2021).
14. Song, W. & Kumar, M. Beyond aquaporins: recent developments in artificial water channels. *Langmuir* **38**, 9085–9091 (2022).
15. Yan, T., Zheng, X., Liu, S., Zou, Y. & Liu, J. Ion transporters: emerging agents for anticancer therapy. *Sci. China Chem.* **65**, 1265–1278 (2022).
16. Dey, S. et al. Quinoline thiourea-based zinc ionophores with antibacterial activity. *J. Med. Chem.* **66**, 11078–11093 (2023).
17. Mondal, A., Ahmad, M., Mondal, D. & Talukdar, P. Progress and prospects toward supramolecular bioactive ion transporters. *Chem. Commun.* **59**, 1917–1938 (2023).
18. He, L., Zhang, T., Zhu, C., Yan, T. & Liu, J. Crown ether-based ion transporters in bilayer membranes. *Chem. Eur. J.* **29**, e202300044 (2023).
19. de Jong, J., Bos, J. E. & Wezenberg, S. J. Stimulus-controlled anion binding and transport by synthetic receptors. *Chem. Rev.* **123**, 8530–8574 (2023).
20. Ahmad, M., Gartland, S. A. & Langton, M. J. Photo- and redox-regulated transmembrane ion transporters. *Angew. Chem. Int. Ed.* **62**, e202308842 (2023).
21. Shen, J., Ren, C. & Zeng, H. Q. Membrane-active molecular machines. *Acc. Chem. Res.* **55**, 1148–1159 (2022).
22. Johnson, T. G. & Langton, M. J. Molecular machines for the control of transmembrane transport. *J. Am. Chem. Soc.* **145**, 27167–27184 (2023).
23. Yuan, X., Shen, J. & Zeng, H. Q. Artificial transmembrane potassium transporters: designs, functions, mechanisms and applications. *Chem. Commun.* **60**, 482–500 (2024).
24. Langton, M. J. Engineering of stimuli-responsive lipid-bilayer membranes using supramolecular systems. *Nat. Rev. Chem.* **5**, 46–61 (2021).
25. Wu, X. et al. Voltage-switchable HCl transport enabled by lipid headgroup–transporter interactions. *Angew. Chem. Int. Ed.* **58**, 15142–15147 (2019).
26. Zhu, J. et al. Reversible ligand-gated ion channel via the interconversion between hollow single helix and intertwined double helix. *Angew. Chem. Int. Ed.* https://doi.org/10.1002/anie.201916755 (2020).
27. Fares, M. et al. Stimuli-responsive cycloaurated "OFF-ON" switchable anion transporters. *Angew. Chem. Int. Ed.* **59**, 17614–17621 (2020).
28. Tapia, L. et al. pH-dependent chloride transport by pseudopeptidic cages for the selective killing of cancer cells in acidic microenvironments. *Angew. Chem. Int. Ed.* **58**, 12465–12468 (2019).
29. Docker, A., Johnson, T. G., Kuhn, H., Zhang, Z. & Langton, M. J. Multistate redox-switchable ion transport using chalcogen-bonding anionophores. *J. Am. Chem. Soc.* **145**, 2661–2668 (2023).
30. Lien, L., Jaikaran, D. C. J., Zhang, Z. & Woolley, G. A. Photomodulated blocking of gramicidin ion channels. *J. Am. Chem. Soc.* **118**, 12222–12223 (1996).
31. Khairutdinov, R. F. & Hurst, J. K. Light-driven transmembrane ion transport by spiropyran–crown ether supramolecular assemblies. *Langmuir* **20**, 1781–1785 (2004).
32. Yang, R.-Y., Bao, C.-Y., Lin, Q.-N. & Zhu, L.-Y. A light-regulated synthetic ion channel constructed by an azobenzene modified hydraphile. *Chin. Chem. Lett.* **26**, 851–856 (2015).
33. Zhou, Y. et al. Reversible photo-gated transmembrane channel assembled from an acylhydrazone-containing crown ether triad. *Chem. Commun.* **53**, 3681–3684 (2017).
34. Salunke, S. B., Malla, J. A. & Talukdar, P. Phototriggered release of a transmembrane chloride carrier from an o-nitrobenzyl-linked pro-carrier. *Angew. Chem. Int. Ed.* **58**, 5354–5358 (2019).
35. Kerckhoffs, A. & Langton, M. J. Reversible photo-control over transmembrane anion transport using visible-light responsive supramolecular carriers. *Chem. Sci.* **11**, 6325–6331 (2020).
36. Ahmad, M., Metya, S., Das, A. & Talukdar, P. A sandwich azobenzene–diamide dimer for photoregulated chloride transport. *Chem. Eur. J.* **26**, 8703–8708 (2020).
37. Wang, W. Z. et al. Light-driven molecular motors boost the selective transport of alkali metal ions through phospholipid bilayers. *J. Am. Chem. Soc.* **143**, 15653–15660 (2021).
38. Wang, C. et al. A light-operated molecular cable car for gated ion transport. *Angew. Chem. Int. Ed.* **60**, 14836–14840 (2021).
39. Wezenberg, S. J. et al. Photomodulation of transmembrane transport and potential by stiff-stilbene based bis(thio)ureas. *J. Am. Chem. Soc.* **144**, 331–338 (2022).
40. Yang, H. et al. A light-driven molecular machine controls K^+ channel transport and induces cancer cell apoptosis. *Angew. Chem. Int. Ed.* **61**, e202204605 (2022).
41. Johnson, T. G., Sadeghi-Kelishadi, A. & Langton, M. J. A photoresponsive transmembrane anion transporter relay. *J. Am. Chem. Soc.* **144**, 10455–10461 (2022).
42. Qu, D.-H., Wang, Q.-C., Zhang, Q.-W., Ma, X. & Tian, H. Photoresponsive host–guest functional systems. *Chem. Rev.* **115**, 7543–7588 (2015).
43. Thaggard, G. C. et al. Metal–photoswitch friendship: from photochromic complexes to functional materials. *J. Am. Chem. Soc.* **144**, 23249–23263 (2022).
44. Li, N. et al. Buckyball-based spherical display of crown ethers for de novo custom design of ion transport selectivity. *J. Am. Chem. Soc.* **142**, 21082–21090 (2020).
45. Ren, C. et al. Molecular swings as highly active ion transporters. *Angew. Chem. Int. Ed.* **58**, 8034–8038 (2019).
46. Ye, R. J. et al. Molecular ion fishers as highly active and exceptionally selective K+ transporters. *J. Am. Chem. Soc.* **141**, 9788–9792 (2019).
47. Zhang, H., Ye, R., Mu, Y., Li, T. & Zeng, H. Q. Small molecule-based highly active and selective K^+ transporters with potent anticancer activities. *Nano Lett.* **21**, 1384–1391 (2021).
48. Shen, J., Han, J. J. Y., Ye, R. J. & Zeng, H. Q. Molecular rotors as a class of generally highly active ion transporters. *Sci. China Chem.* **64**, 2154–2160 (2021).
49. Sueishi, Y. & Hishikawa, H. Complexation of 4-dimethylaminoazobenzene with various kinds of cyclodextrins: effects of cyclodextrins on the thermal cis-to-trans isomerization. *Int. J. Chem. Kinet.* **34**, 481–487 (2002).
50. Moore, S. S., Tarnowski, T. L., Newcomb, M. & Cram, D. J. Host-Guest Complexation. 4. Remote Substituent Effects on Macrocyclic Polyether Binding to Metal and Ammonium Ions. *J. Am. Chem. Soc.* **99**, 6398–6405 (1977).

Acknowledgements

This work is supported by the National Natural Science Foundation of China (22371048 to J.S. and 22271049 to H.Z.) and Natural Science Foundation of Fujian Province (2023J01054 to J.S.), The "Chu Ying Program" for the Top Young Talents of Fujian Province to J.S., and a start-up grant from Fuzhou University to H.Z.

Author contributions

Z.L. performed the synthesis and host-guest complexation. L.Y. performed ion transport study. W.C. and J.L. contributed to molecular

modeling. J.S. and H.Z. conceived and supervised the project and wrote the manuscript. All authors participated in discussion and editing of the manuscript.

Competing interests
The authors declare no competing interests.

Additional information
Supplementary information The online version contains supplementary material available at https://doi.org/10.1038/s41467-025-62113-1.

Correspondence and requests for materials should be addressed to Jie Shen or Huaqiang Zeng.

Peer review information *Nature Communications* thanks the anonymous reviewers for their contribution to the peer review of this work. A peer review file is available.

Reprints and permissions information is available at http://www.nature.com/reprints

Publisher's note Springer Nature remains neutral with regard to jurisdictional claims in published maps and institutional affiliations.

Open Access This article is licensed under a Creative Commons Attribution-NonCommercial-NoDerivatives 4.0 International License, which permits any non-commercial use, sharing, distribution and reproduction in any medium or format, as long as you give appropriate credit to the original author(s) and the source, provide a link to the Creative Commons licence, and indicate if you modified the licensed material. You do not have permission under this licence to share adapted material derived from this article or parts of it. The images or other third party material in this article are included in the article's Creative Commons licence, unless indicated otherwise in a credit line to the material. If material is not included in the article's Creative Commons licence and your intended use is not permitted by statutory regulation or exceeds the permitted use, you will need to obtain permission directly from the copyright holder. To view a copy of this licence, visit http://creativecommons.org/licenses/by-nc-nd/4.0/.

© The Author(s) 2025